Journal of Marine Research, 58, 37–60, 2000

The stability of an *NPZ* model subject to realistic levels of vertical mixing

by Christopher A. Edwards[1,2], Thomas A. Powell[1] and Harold P. Batchelder[1]

ABSTRACT

The linear stability of a vertically-distributed, Nutrient-Phytoplankton-Zooplankton (*NPZ*) ocean ecosystem model is analyzed to understand how vertical mixing influences biological dynamics. In the absence of vertical diffusion, the model generally exhibits both stable fixed point and limit cycle behavior, depending on the depth and choice of parameters. Diffusion couples the dynamics of nearby levels and can induce stable profiles as well as oscillatory dynamical trajectories that become vertically phase-locked for large mixing levels. Calculations of the Lyapunov exponent reveal that vertical diffusion can drive this model into a chaotic state, though this occurs only for levels of diffusion well below those found in nature. The dynamics of the model, assuming macrozooplankton are the dominant grazers in the ecosystem, are compared to those in which microzooplankton dominate, with a faster grazing rate and poor assimilation efficiency. While the coupled physical-macrozooplanton system has a stable profile, the coupled microzooplankton profile remains unstable, even at large mixing levels. Fluctuations occur on time scales varying between a few days and a few months, depending on the parameters and magnitude of diffusion.

1. Introduction

Many models that describe the interaction between different plankton taxa in the ocean have been formulated and applied to studies of pelagic ecosystems. One class of such models includes the box models that group entire populations into individual, mutually interacting compartments. Complexity in these models varies widely, depending on the number of state variables included as well as the rules that govern their interaction. One well-known model (Fasham *et al.,* 1990) includes seven boxes: phytoplankton, zooplankton, bacteria, nitrate, ammonium, dissolved organic nitrogen, and detritus. Among the most simple of the prognostic biological models is the *NPZ* model of Franks *et al.* (1986), which considers only three compartments: phytoplankton, zooplankton, and dissolved nutrients.

Although the number of components and the details of process formulations vary, each model has been used to simulate and, in turn, interpret the development of phytoplankton blooms and other biological features in the ocean. The models are often coupled to physical

1. 3060 VLSB, Department of Integrative Biology, University of California, Berkeley, California, 94720-3140, U.S.A.

2. Present address: University of Connecticut, Department of Marine Sciences, 1084 Shennecossett Road, Groton, Connecticut, 06340-6097, U.S.A.

models of different levels of complexity. Examples of zero-dimensional ecosystem models (in which biological fields are averaged over the surface mixed layer) include those of Fasham *et al.* (1990) and Denman and Gargett (1995). Doney *et al.* (1996) coupled a multi-component biological model with a one-dimensional (vertical) physical model to reproduce chlorophyll features observed at the Bermuda Atlantic Time-Series (BATS) Site. In two dimensions, Wroblewski (1977) modeled the development of phytoplankton blooms along the Oregon coast during upwelling-favorable wind conditions. When coupled to large-scale general circulation models, the large-scale geographical distribution of climatological primary productivity can also be assessed (e.g., Sarmiento *et al.,* 1993).

Even as these models are increasingly applied to a variety of physical circumstances, a fundamental understanding of their underlying dynamics remains incomplete. Such understanding is essential to their interpretation. Individual simulations are simply incapable of characterizing the system. Collections of simulations often explore model result sensitivity to reasonable changes in poorly known parameters. In some studies, the steady state solution is determined and its sensitivity to parameter choices calculated (e.g., Moisan and Hofmann (1996) for a one-dimensional physical/biological model). In general, though, the dynamics of that steady solution are not analyzed.

The model of Franks *et al.* (1986) represents a counter-example, a model which has been well characterized in zero physical dimensions. In the original work, the authors determined the analytic steady-state solutions and compared the temporal response and parameter sensitivity of the model using both an Ivlev and an alternative Mayzaud-Poulet grazing function for a given set of parameters. Subsequently, Busenberg *et al.* (1990) performed a detailed analysis of the existence and stability of the model's steady-state solutions. Both stable and unstable fixed points, resulting in limit cycle oscillations, were noted for solutions with nonzero phytoplankton, zooplankton and nutrient concentrations. However, the dynamics of the biological system are inherently spatially dependent because the growth rate is naturally dependent on the light field which decays with depth. As a result, the dynamics should be expected to vary within the water column, even in the absence of physical processes.

Furthermore, physical mechanisms may significantly impact the dynamics of the biological fields. The contribution of vertical mixing toward setting physical properties in the surface ocean is well established. Wind, thermal, and fresh-water forcing at the surface drives turbulent structures that mix physical properties vertically and in turn influence the exchange of momentum, heat and fresh water between the atmosphere and the ocean. The calculation of the depth of the mixed layer and the magnitude of the mixing coefficient are critical components of physical models and not surprisingly also affect the development of biological fields. Indeed, it is the interaction of vertical mixing and biological processes that forms the foundation of the seminal theory of plankton blooms (Sverdrup, 1953). The significant role that the mixed layer plays in the growth and structure of phytoplankton patches has been described by Franks (1997). In that work, a coupled bio-physical model examined cross-frontal exchange with and without surface mixed-layer models. Both a

slab mixed-layer model and a turbulence-closure scheme were tested and, though the systems were complicated by the inclusion of advective effects, the vertical mixing was shown to strongly influence the magnitude and physical scales of the evolving patches as well as their nonlinear interactions. By redistributing material vertically, diffusion modifies the dynamical budgets and can lead to substantially different time series than would be expected in its absence.

This paper builds upon previous efforts by exploring the effects of vertical diffusion on the dynamics of the simple second-order biological model of Franks *et al.* (1986). This is of interest for two primary reasons. First, although simple, this model has been widely applied to several ocean systems, ranging from basin scale (Wroblewski *et al.,* 1988) to more localized wind-forced (Franks and Walstad, 1997) and tidally forced (Franks and Chen, 1996) frontal systems. Despite its wide application, a detailed analysis of the model response to vertical mixing has not been explored. We do that here. Second, the model as it has been generally applied has had parameter values suited to macrograzers (copepods). Within the past 15 years, numerous studies (Gifford, 1988; Banse, 1992; Verity *et al.,* 1993; Neuer and Cowles, 1994) have documented that the primary grazers in almost all ocean ecosystems are not the copepods, but rather the microzooplankton. Microzooplankton, particularly ciliates and heterotrophic flagellates, have biological dynamics very different from copepods. Without altering the fundamental configuration of the model, we reparameterize the grazing component of the *NPZ* model to better represent known microzooplankton dynamics/bioenergetics, evaluate the response of the "microzooplankton" model to vertical mixing and compare it to the "macrozooplankton" model. We conduct the analysis in a stepwise fashion, first in the absence of physical processes, and then with the addition of vertical diffusion. We examine the potential stabilizing and destabilizing impact of vertical mixing on the coupled bio-physical system. Depending on the parameter set and the magnitude of the diffusion, the dynamics can be either stabilized or destabilized. In some cases, the influence is found to be nonmonotonic. That is, moderate diffusivity can stabilize the vertical profile from its heterogeneous nondiffusive character, and yet higher levels lead to oscillations. Lastly, we inquire whether this model generates chaotic plankton dynamics. The existence of chaos in pelagic ecosystems remains an open research question. Model studies (e.g., Hastings and Powell, 1991) suggest that ecosystem dynamics may be chaotic, and limited observational evidence (e.g., Ascioti *et al.,* 1993) supports deterministic nonlinear, though not definitively chaotic, interactions. This aspect of the present model has not been examined, and is of particular interest as such complex behavior could only result from the coupled bio-physical nature of this system. Chaos driven by diffusive coupling of adjacent oscillators was first explored in a spatially-extended predator-prey model by Pascual (1993). For both micro- and macrozooplankton cases, we find that very weak levels of diffusion lead to a chaotic state. However, for realistic levels of mixing associated with internal wave processes, the model does not exhibit chaos.

2. Model formulation

The biological model considers the exchange of nitrogen between single phytoplankton (P) and zooplankton (Z) species, and a nutrient pool (N). The biological interactions are described by

$$\frac{dP}{dt} = \frac{V_m NP}{k_s + N} e^{k_{ext} z} - R_m Z(1 - e^{-\Lambda P}) - mP \tag{2.1a}$$

$$\frac{dZ}{dt} = (1 - \gamma) R_m Z(1 - e^{-\Lambda P}) - gZ \tag{2.1b}$$

$$\frac{dN}{dt} = -\frac{V_m NP}{k_s + N} e^{k_{ext} z} + \gamma R_m Z(1 - e^{-\Lambda P}) + mP + gZ. \tag{2.1c}$$

Here, V_m is the maximum uptake rate of nutrients by the phytoplankton and k_s is the Michaelis-Menten half-saturation value. The uptake is governed by the exponential decay of photosynthetically available radiation below the surface with an e-folding scale of k_{ext}^{-1}. The grazing is assumed to have an Ivlev functional form, with R_m the maximum rate, and Λ sets the level of saturation. The assimilation efficiency of the grazers is denoted $(1 - \gamma)$ and the phytoplankton and zooplankton mortalities are m and g, respectively.

In the ocean, the purely biological dynamics are subject to advection and diffusion. In addition, the total nitrogen within the system is fixed (i.e., $N + P + Z = N_T$). For uniform, N_T, the three component dynamics may be reduced to two and expressed

$$\frac{\partial P}{\partial t} + \mathbf{u} \cdot \nabla P = F + \frac{\partial}{\partial z}\left(K_v \frac{\partial P}{\partial z}\right) + \nabla_h \cdot (K_h \nabla_h P) \tag{2.2a}$$

$$\frac{\partial Z}{\partial t} + \mathbf{u} \cdot \nabla Z = G + \frac{\partial}{\partial z}\left(K_v \frac{\partial Z}{\partial z}\right) + \nabla_h \cdot (K_h \nabla_h Z) \tag{2.2b}$$

where $F = dP/dt$ and $G = dZ/dt$ in the absence of diffusion (i.e., Eqs. 2.1a and 2.1b). Cartesian coordinates (x, y, z) and corresponding velocities (u, v, w) are assumed. The origin is located at the ocean surface, with $z < 0$ within the domain. Though risking some confusion, we apply the conventional notation that small z refers to distance and capital Z refers to the zooplankton concentration. Mixing is anisotropic, K_v being the vertical diffusivity and K_h being its horizontal value. The horizontal gradient operator is denoted by ∇_h.

Our primary concern is the effect of vertical mixing on the dynamics of the model. As a result, we neglect horizontal dimensions (i.e., set $K_h = 0$), set the velocity field to zero, and recast the dynamics in terms of vertical mixing only. The stability of the steady-state solution (P^*, Z^*) is then determined by analyzing the response of small perturbations about the fixed point. Thus we let

$$P(z, t) = P^*(z) + P'(z, t) \tag{2.3}$$

and introduce

$$P'(z, t) = \hat{P}(z)e^{\lambda t}. \tag{2.4}$$

Inserting Eqs. 2.3 and 2.4 into the system 2.2a–2.2b and linearizing then yields the relation

$$\begin{bmatrix} \dfrac{\partial F}{\partial P} + \dfrac{\partial}{\partial z}\left(K_v \dfrac{\partial}{\partial z}\right) & \dfrac{\partial F}{\partial Z} \\ \dfrac{\partial G}{\partial P} & \dfrac{\partial G}{\partial Z} + \dfrac{\partial}{\partial z}\left(K_v \dfrac{\partial}{\partial z}\right) \end{bmatrix} \begin{bmatrix} \hat{P} \\ \hat{Z} \end{bmatrix} = \lambda \begin{bmatrix} \hat{P} \\ \hat{Z} \end{bmatrix}. \tag{2.5}$$

The components of the matrix on the left-hand side of Eq. 2.5 are determined at the fixed point ($P^*(z)$, $Z^*(z)$). If all eigenvalues, λ, have negative real parts then the steady-state solution is linearly stable, whereas one eigenvalue with a positive real part indicates that small perturbations from the solution will grow.

In this work, the fixed point solutions are determined in two steps. First, the steady-state in the absence of diffusion is determined through the analytic solution of Franks *et al.* (1986) over the full domain $-H < z < 0$. Second, this initial condition is iteratively adjusted to approach the solution to the discretized nonlinear set of equations that include nonzero diffusivity. No flux boundary conditions are enforced at the upper and lower boundaries:

$$K_v \frac{dP}{dz} = K_v \frac{dZ}{dz} = 0 \qquad \text{at } z = 0 \text{ and } z = -H. \tag{2.6}$$

The numerical algorithm applied is fsolve.m, included in the Optimization Toolbox of Matlab 5.2 (Mathworks, Inc). We require time-derivative terms associated with the final solution to be smaller than 10^{-4} μmole Nitrogen/(1 day), which is deemed close enough to the true solution for the stability calculations. Most solutions have time-derivatives several orders of magnitude smaller. Once the fixed point is determined, Eq. 2.5 is solved using the eigenvalue solver, eig.m, also included in the standard Matlab distribution. Edwards and Pedlosky (1998) have used this method previously to examine the enhanced barotropic instability of the western boundary current. For this study, $H = 65$ m and $dz = 1$ m. While qualitatively, the behavior described below is quite robust, some quantitative changes occur with differing resolutions. We choose $dz = 1$ m as a reasonable resolution for one-dimensional studies. However, we emphasize that the stability boundaries will vary somewhat for other resolutions and maximum depths. The full system of equations is extended from $n = 2$ for the purely biological model to $n = 2H/dz$ for that including vertical mixing. It is this extension of the dimensionality of the system that enables more complicated dynamics than would occur in the purely biological model.

To facilitate comparisons with other parameter sets, this model can be rescaled through the substitutions described in Table 1 to yield a nondimensional set of equations. Including vertical mixing and dropping primes that represent nondimensional quantities, these

Table 1. Transformations to nondimensionalized model. Nondimensional quantities are denoted with primes.

$$
\begin{aligned}
t' &= V_m t \\
z' &= k_{ext} z \\
P' &= P/N_T \\
Z' &= Z/N_T \\
N' &= N/N_T \\
R'_m &= R_m/V_m \\
m' &= m/V_m \\
g' &= g/V_m \\
k'_s &= k_s/N_T \\
\Lambda' &= N_T \Lambda \\
K'_v &= K_v \frac{k_{\text{ext}}^2}{V_m} \\
\gamma' &= \gamma
\end{aligned}
$$

equations are expressed

$$\frac{dP}{dt} = \frac{NP}{k_s + N} e^z - R_m Z(1 - e^{-\Lambda P}) - mP + K_v \frac{\partial^2 P}{\partial z^2} \tag{2.7a}$$

$$\frac{dZ}{dt} = (1 - \gamma) R_m Z(1 - e^{-\Lambda P}) - gZ + K_v \frac{\partial^2 Z}{\partial z^2}. \tag{2.7b}$$

As our interest is to examine the influence of realistic mixing levels on the *NPZ* dynamics, all results expressed in this study are dimensional. All times and rates cited are in terms of days and meters, except for diffusivities which are always cast in the more conventional m^2/s. The nondimensional values can be obtained easily by scaling time by the uptake rate inverse, V_m^{-1}, depth by the light-limiting *e*-folding scale, k_{ext}^{-1}, and the biomass concentrations by the total nitrogen, N_T.

In the next section, we compare and contrast two parameter sets defined in Table 2. Set (a) represents the more conventional parameters used in Franks and Walstad (1997). In particular, the parameters related to the growth efficiency, the maximum grazing rate R_m, the Ivlev constant Λ and the assimilation efficiency $(1 - \gamma)$, are most applicable to a system in which macrozooplankton, like copepods, are the primary grazers. These parameter choices reflect the longstanding bias in the ocean ecosystem modeling community to ignore the micrograzers, and to assume a nutrient-diatom-copepod system. Over the past 15 years many studies have documented that microzooplankton—ciliates and flagellates—are the predominant grazers in both nearshore and oceanic ecosystems (Gifford, 1988; Banse, 1992; Verity *et al.,* 1993; Neuer and Cowles, 1994). Microzooplankton have very different biological dynamics than copepods. First, protists undergo cell division, so their numerical response to favorable feeding conditions is rapid and not limited by

Table 2. Biological parameters applied in this study. Set (a) is targeted toward macrozooplankton grazers, and set (b) corresponds to microzooplankton-dominated systems.

	(a) Macro	(b) Micro	Units
V_m	2.0	2.0	day^{-1}
k_s	0.1	0.1	μmole Nitrogen l^{-1}
k_{ext}	0.06	0.06	m^{-1}
R_m	0.5	4.0	day^{-1}
Λ	0.2	0.3	(μmole Nitrogen $l^{-1})^{-1}$
γ	0.3	0.7	
m	0.1	0.1	day^{-1}
g	0.2	0.2	day^{-1}
N_T	10	10	μmole Nitrogen l^{-1}

life-history constraints. Growth rates for microzooplankton rival those of their phytoplankton prey, on the order of 0.5–2.0 day^{-1} (Strom and Morello, 1998). Assuming gross growth efficiency (growth/ingestion) of micrograzers to be roughly 0.33 (range 0.15–0.64; Strom and Morello, 1998; Straile, 1997), then ingestion must be of order 1.5–6.0 day^{-1}—clearly sufficient to consume large quantities of phytoplankton and prevent substantial blooms. If a third of the consumed phytoplankton contributes to zooplankton biomass, then the remainder is immediately remineralized (through excretion and metabolism) to the dissolved nutrient pool. In short, microzooplankton efficiently convert phytoplankton biomass into dissolved nutrients, while macrozooplankton convert phytoplankton predominantly into zooplankton biomass, and only slowly into dissolved nutrients. Thus, microzooplankton- and macrozooplankton-dominated ecosystems (and models) differ dramatically in the relative flows between the *NPZ* compartments. To explore these *Z*-compartment differences (ingestion, growth, remineralization), we altered three parameters in the *NPZ* model (Table 2, set (b)). The microzooplankton parameterization has a maximum ingestion rate R_m that is eight times higher than that of macrozooplankton. Second, we increased Λ by 50%, which causes grazing in the microzooplankton to saturate at lower levels of phytoplankton. And finally, we more than doubled γ, so that more of the ingested phytoplankton is remineralized than incorporated into zooplankton biomass.

3. Results

a. Dynamics without diffusion

The linearized model, Eq. 2.5, is examined initially in the absence of diffusion by setting $K_v = 0$. This simplification eliminates the coupling between vertical levels. Biological interactions at each level can now be considered independent dynamical systems having different maximal uptake rates equal to $V_m \times e^{k_{ext}z}$. The steady solutions of this system have been described by Wroblewski *et al.* (1988) and their existence and stability carefully characterized by Busenberg *et al.* (1990).

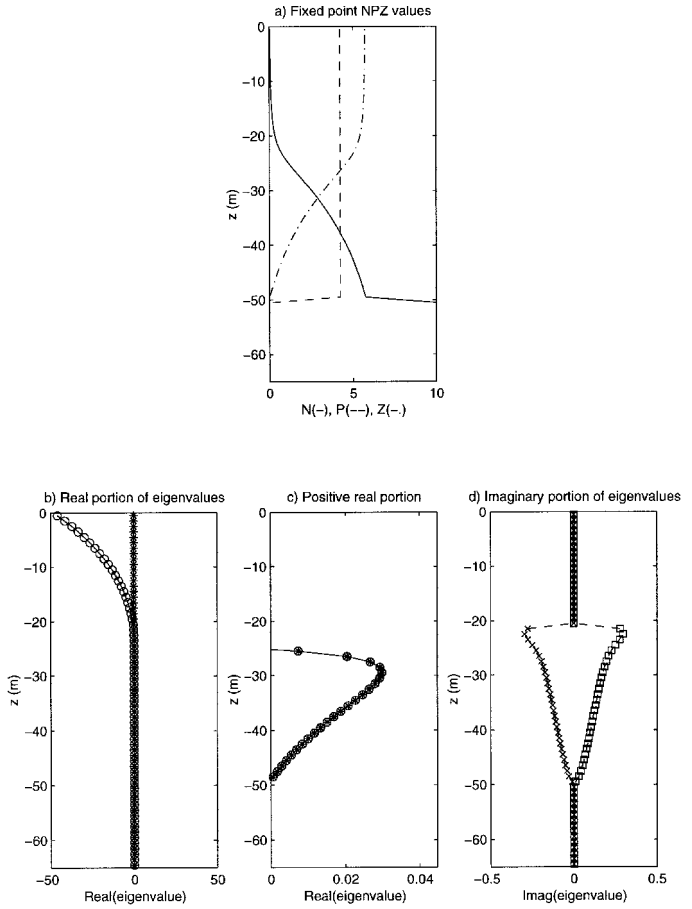

Figure 1. Steady profile and eigenvalues for the macrozooplankton parameters and zero diffusion. (a) Steady-state solution for N (−), P (--), and Z(−·) which results in eigenvalues whose real portion is shown in (b) and positive real portion emphasized in (c). The imaginary component is shown in (d). N, P, and Z are expressed in μmole Nitrogen/l and eigenvalues are expressed in units day^{-1}.

For the macrozooplankton parameterization, the fixed point solution and eigenvalues are shown in Figure 1. The steady state solution shown in Figure 1a, which was also determined in Franks and Walstad (1997), can be divided into two domains. Above a transition depth (roughly $z = -50$ m for this parameter set), there exists a solution with nonzero phytoplankton and zooplankton components. In this region, the phytoplankton population is independent of depth, depending only on the grazing and zooplankton mortality parameters through Eq. 2.1b, and not on the magnitude of the uptake. Below this depth, a steady solution with zero phytoplankton and zooplankton concentrations applies. To be precise, the transition depth itself really represents a narrow window within which a steady solution balancing only phytoplankton and nutrients is found. However, on the

coarse resolution of the present model, this balance is not observed, and as a result is ignored in our further discussion.

Presented in Figure 1b is the real portion of the eigenvalues associated with this steady-state solution, two eigenvalues at each depth level. Near the surface, the set of the eigenvalues marked with the circles have large negative real parts. Eigenvalues denoted by stars are also negative near the surface, though barely so with values near -0.2/day. These values indicate that the steady solution near the surface is stable. At mid-depth, the sign of the eigenvalues is difficult to interpret, and as a result, we plot in Figure 1c the same eigenvalues as in Figure 1b, but only show the positive half-plane. Though of smaller magnitude than the negative values near the surface, there clearly exists a portion of the water column (between 25 and 50 m) with eigenvalues having positive real parts. At these depths the steady state is linearly unstable. Finally, at depths below $\sim$50 m, the steady solution, with zero phytoplankton and zooplankton concentrations, is again stable. The dynamical modes are further characterized by the imaginary portion of the eigenvalue, shown in Figure 1d. Here, the near-surface eigenvalues have zero imaginary part, indicating a direct return to the stable fixed point. In the unstable portion of the water column, the eigenvalues have nonzero imaginary components. In fact, they are complex conjugate solutions, since the matrix in Eq. 2.5 is real. Thus the solution will drift away from the steady states in an oscillatory fashion, ultimately leading to limit cycle behavior because individual pools of nitrogen are necessarily bounded by the total magnitude of nitrogen N_T in the system. Finally, in the biologically stable depths below 50 m, the eigenvalues are purely real, reflecting again a direct return to the stable fixed points. We also note that there exists a narrow set of depths just above the unstable region in which the eigenvalues have negative real part, but are complex. At these depths, the model should return to the stable state through an oscillatory exchange of nitrogen between the three pools.

To illustrate the utility of the fixed-point analysis in describing the dynamical response of the model, we show in Figure 2 time series of N, P, and Z, at several depths for the nondiffusive, macrozooplankton parameter system. In each panel, the model was initialized at levels, $P = 4$ μmole Nitrogen/l and $N = Z = 3$ μmole Nitrogen/l. Each of the different regimes described above can be observed. In the uppermost panel, corresponding to a 5-m depth, the system returns following a transient phytoplankton bloom to its stable equilibrium near the surface. In panel (b) at 25 m, the return is through oscillations with a period of approximately 25 days. At 35-m depth in panel (c), the system approaches limit cycles with oscillations over roughly 50 days. We do not expect the time scale for oscillation predicted by the stability analysis to apply exactly to the system far from equilibrium because the analysis specifically characterizes only small perturbations from that steady state; however, it is worth comparing these estimates quantitatively. The imaginary component of the eigenvalue at 25 m depth is approximately $Im(\lambda) = 0.25$/day, which corresponds to a period of oscillation of $T = 2\pi/Im(\lambda) \cong 25$ days. The quantitative agreement at 45 m depth is not as good, though the qualitative trend is borne out by the stability analysis: $Im(\lambda) = 0.064$/day, which implies a period $T \cong 98$ days. Though not

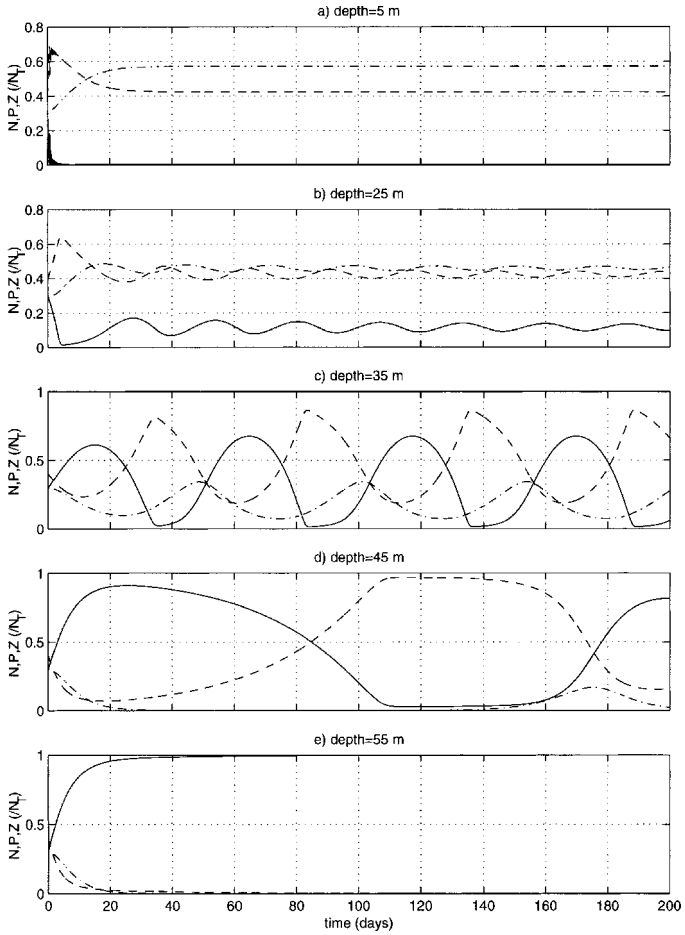

Figure 2. Time series solution of the nondiffusive macrozooplankton model at depths (a) 5 m, (b) 25 m, (c) 35 m, (d) 45 m, and (e) 55 m. Nutrients are shown as solid, phytoplankton as dashed, and zooplankton is shown as dot-dashed lines.

shown, a longer time series at 45 m reveals oscillations with a period of roughly 125 days. Finally, the return to the stable phytoplankton- and zooplankton-free equilibrium at $z =$ 55 m is presented in Figure 2e.

Applying the same analysis to the microzooplankton parameterization (Table 2, column b) illustrates that the structure of dynamical behavior associated with the macrozooplankton parameters is not universal, but can vary with the parameters chosen. Figure 3a shows the steady state profile for the microzooplankton. The same basic structure exists with nonzero phytoplankton and zooplankton values only above the transition depth (which is the same as the previous case because the parameters which determine this depth have not changed). However, the magnitude of the phytoplankton and zooplankton is now consider-

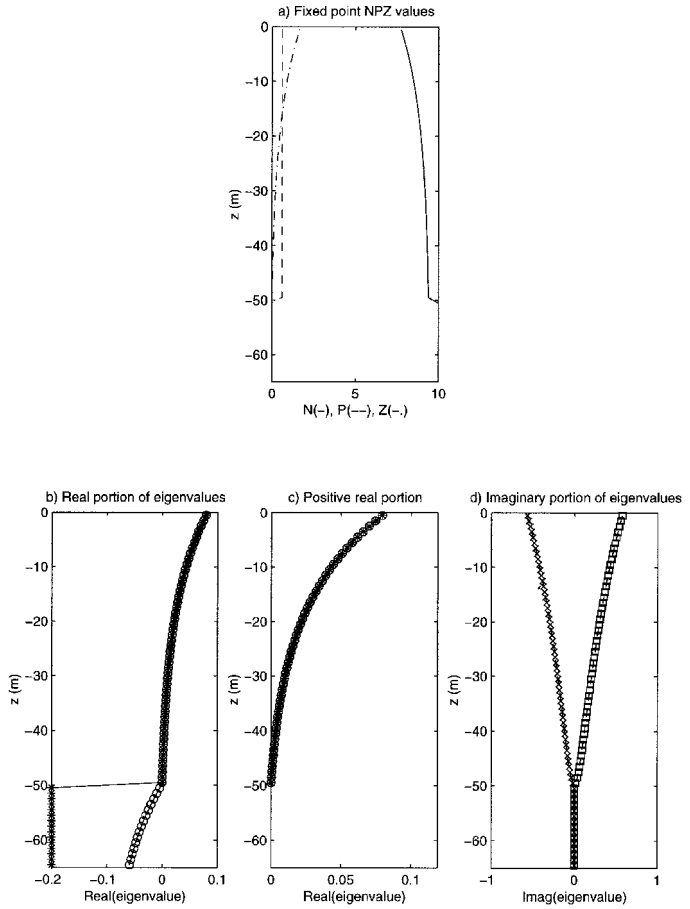

Figure 3. Steady profile and eigenvalues as in Figure 1, for the microzooplankton parameters in the absence of diffusion: (a) Steady-state solution for N (−), P (--), and Z(−·); (b) real portion of associated eigenvalues; (c) positive real portion; (d) imaginary component.

ably smaller than in the previous case. There is little nutrient depletion in the surface waters with this steady solution. The phytoplankton levels are determined through a balance of assimilated ingestion and zooplankton mortality. The substantial increase in the grazing constants of the microzooplankton parameterization leads directly to this reduction in the steady-state value. As before, eigenvalues are real and negative below the transition depth. However, above this depth, all eigenvalues are complex, with positive real parts. Thus the steady solution is unstable to small perturbations at all depths above roughly $z = -50$ m. The time series of N, P and Z shown in Figure 4 again confirms expectations from the linear stability analysis. For all levels above the transition depth, the microzooplankton model exhibits limit cycle behavior, with the period of oscillation increasing with depth.

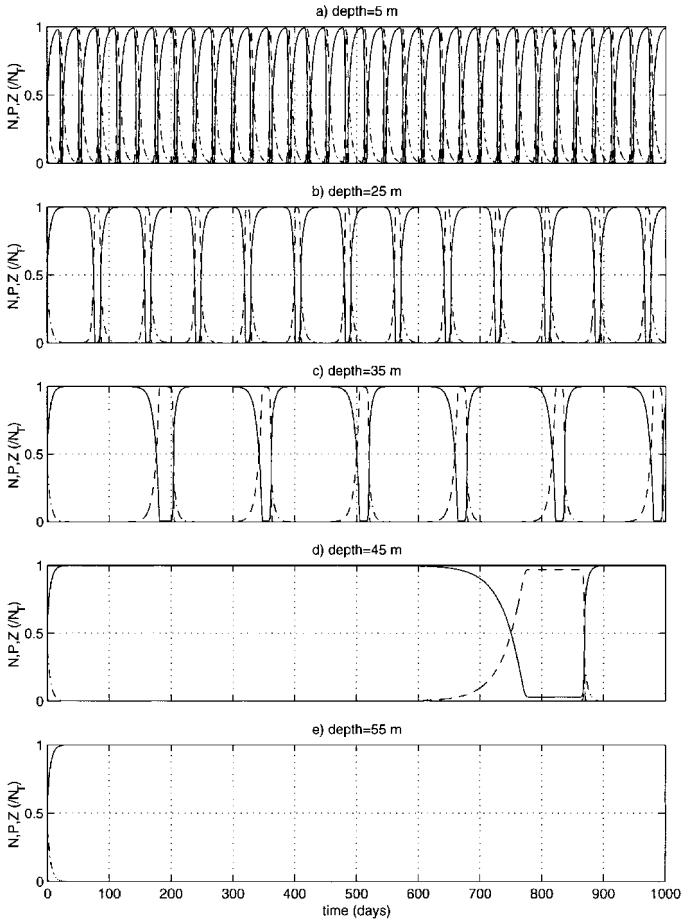

Figure 4. As in Figure 2, time series solution of the nondiffusive microzooplankton model at depths (a) 5 m, (b) 25 m, (c) 35 m, (d) 45 m, and (e) 55 m.

b. Dynamics with diffusion

i. Linear stability. The limited range of behavior observed in the previous section is to be expected in second-order dynamical systems. As shown below, this behavior is enriched through the coupling of diffusion which multiplies the dimension by the number of levels. Thus dynamics otherwise impossible in such a simple biological system are observed.

Figure 5a shows the steady-state solution subject to vertical diffusion corresponding to background, internal wave levels of the deep ocean ($K_v = 10^{-5}$ m^2/s) (Toole *et al.,* 1994; Polzin *et al.,* 1997). The close similarity of this fixed point to the analytical solution of Figure 1a is clear. In the upper portion of the water column there is very little modification to the profile. The major difference occurs near the transition depth where the analytic profile is discontinuous. Diffusion modifies the steady solution to one with smooth

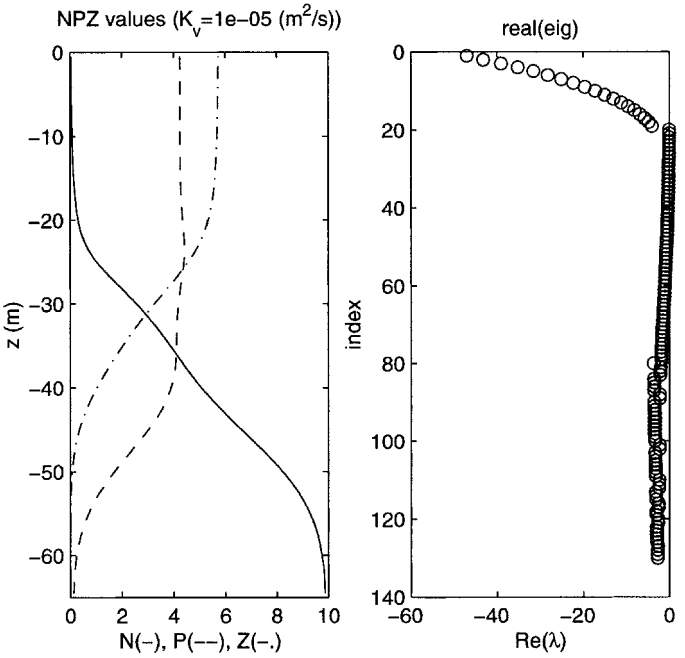

Figure 5. (a) The fixed point solution (N (—), P (--), and Z(—·)) subject to $K_v = 10^{-5}$ m^2/s and (b) real part of the eigenvalues for the macrozooplankton parameters. All eigenvalues have real parts less than zero. N, P, and Z are expressed in μmole Nitrogen/l and eigenvalues are expressed in units day^{-1}.

gradients. Panel 5b shows the real parts of eigenvalues associated with this steady solution. Unlike the analogous previous plots in which depth was used as the vertical axis, these real parts are plotted as a function of an index associated with an arbitrary numbering of the eigenvalues. This index serves to connect each growing or decaying mode with its vertical structure as given by the corresponding eigenfunction, to be explored further below. It is clear from Figure 5b that there again exist a series of decaying modes, with very large amplitude, as in the nondiffusive system. However, close examination of the eigenvalues reveals that none has positive real part. The linear stability analysis suggests that diffusion has stabilized the fixed point solution.

The temporal progression of the coupled system at several depths is shown in Figure 6. In the surface waters, there exists the same phytoplankton bloom, followed by a slow (~30 day) return to equilibrium values. At formerly unstable mid-depths the fields return to equilibrium, as a damped oscillator, consistent with complex eigenvalues (not presented). The time scale for the mid-depth return to equilibrium is approximately 70 days. Indeed, diffusion does stabilize this biological profile.

In a similar calculation of the modes using a higher level of diffusivity ($K_v = 10^{-2}$ m^2/s), all resulting eigenvalues have a negative real part, as in the case just examined. However, at this higher level of mixing all eigenvalues are real, implying a direct return to equilibrium

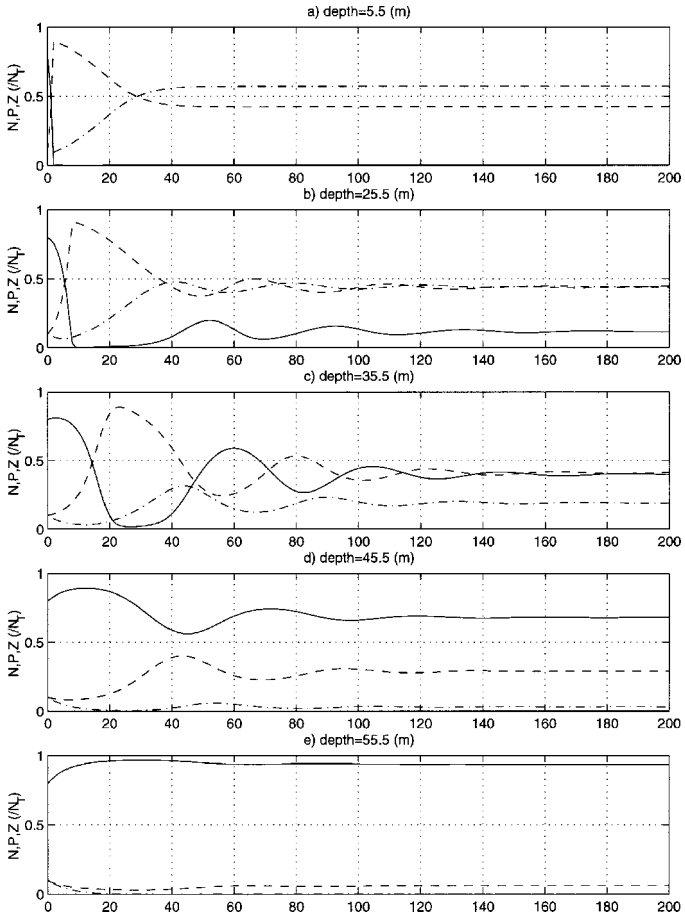

Figure 6. As in Figure 2, but with time series solution of the diffusive macrozooplankton model ($K_v = 10^{-5}$ m^2/s) at depths (a) 5.5 m, (b) 25.5 m, (c) 35.5 m, (d) 45.5 m, and (e) 55.5 m.

at all depths. This behavior is borne out in the time series shown in Figure 7, in which the strong vertical mixing leads to nearly uniform dynamics within the water column. The steady state approached varies in the vertical, but the initial phytoplankton blooms, followed by their relaxation to equilibrium all have the same time scale. Thus for this parameter set, diffusion stabilizes the water column and does so more strongly at higher levels of mixing, with slow oscillatory returns at weak levels and more direct and vertically coupled returns at higher levels.

In the limit of very weak mixing, the diffusive model (Eq. 2.5) must be consistent with the nondiffusive model described above. Calculations at a range of mixing levels indicate that the transition from an unstable mid-depth part of the water column to stability occurs for this parameter set at approximately 3.9×10^{-7} m^2/s, well below diffusivities found in nature.

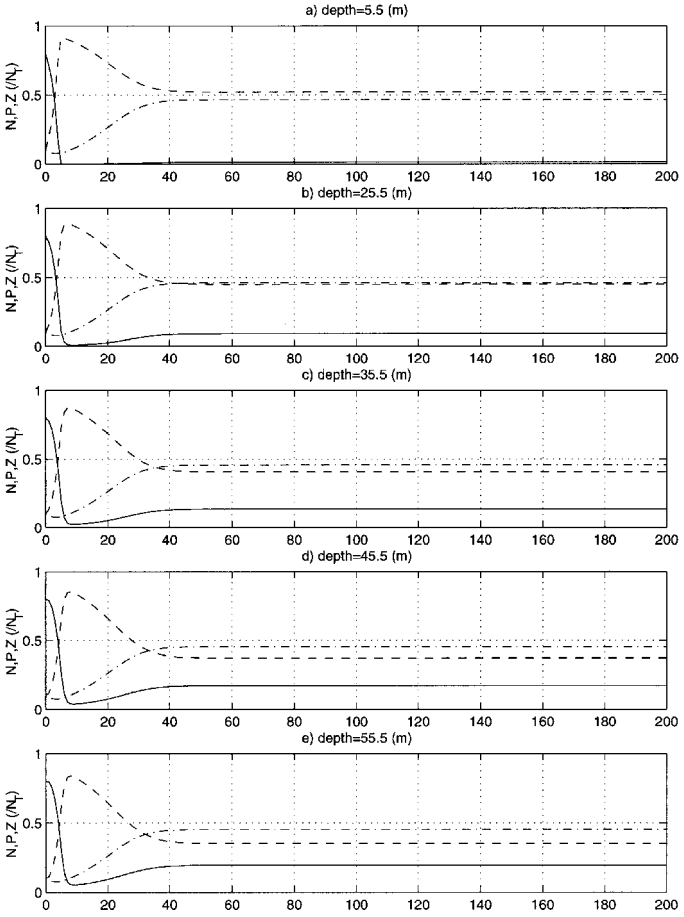

Figure 7. As in Figure 6, with time series solution of the diffusive macrozooplankton model but with $K_v = 10^{-2}$ m^2/s.

This stabilizing effect of mixing is not universal, and can be explored further through the microzooplankton model. As described above the nondiffusive case reveals linearly unstable, steady-state solutions throughout the upper 50 m of the water column with the maximum growth rate nearest the surface. As before, mixing couples biological dynamics in the vertical. However, for diffusivities up to 10^{-2} m^2/s, the model remains unstable. Figure 8 shows the stability properties for $K_v = 10^{-5}$ m^2/s. The vertical profile of the steady solution shown in panel (a) reveals some modification of the nondiffusive steady solution near the transition depth. In panel (b) is shown only the positive real part of the eigenvalues. There are two growing modes, and they are complex conjugate solutions with their imaginary parts shown in panel (c). The vertical structure of this growing mode is shown in panel (d) for the phytoplankton field and (e) for the zooplankton. Each eigenfunction shows a surface-enhanced amplitude function.

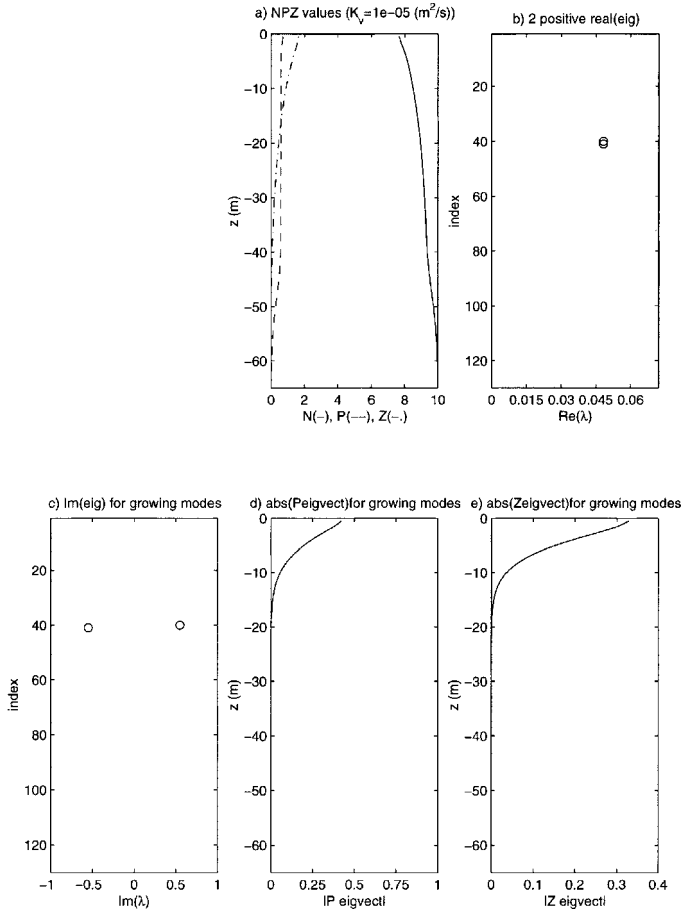

Figure 8. Steady profile, eigenvalues and structure of growing modes for the microzooplankton diffusive model ($K_v = 10^{-5}$ m^2/s): (a) the steady solution; (b) positive real eigenvalues; (c) imaginary components of eigenvalues shown in (b); the eigenvectors of growing modes for phytoplankton (d) and for zooplankton (e). N, P, and Z are expressed in μmole Nitrogen/l and eigenvalues are expressed in units day^{-1}.

The dynamics alter little for increased mixing levels (not shown). Growing modes are found for all diffusivities tested up to a level of $K_v = 10^{-2}$ m^2/s. The main differences at higher diffusivities are, not surprisingly, that the steady solutions and eigenfunctions become more vertically uniform and less surface enhanced. This fact is reflected in the time series. At the background mixing levels, the time-scales of the oscillations vary with depth. However, at larger levels, the variability becomes phase-locked in the vertical. Finally, it is worth noting that the time scales of the variability reflect not the surface values of the nondiffusive system, but rather a growth rate at an intermediate depth. The oscillations

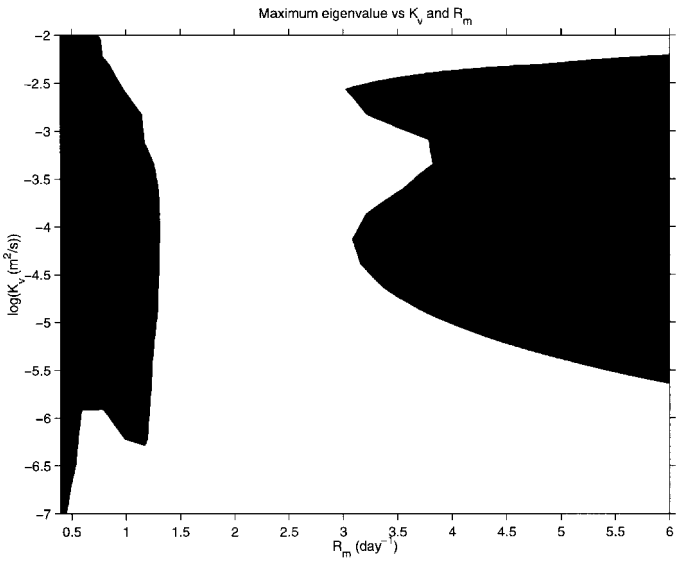

Figure 9. Stability diagram for the macrozooplankton model parameters subject to variable diffusion and maximum grazing rate. Dark portions indicate stable regions in which the largest real part of the eigenvalues is negative. The light portion indicates linearly unstable regions.

have roughly a 50-day period, roughly twice that of the surface oscillations in the nondiffusive limit.

The previous analysis can be applied to efficiently scan parameter space. Since it is the sign of the real part of the eigenvalues that determines the return to or motion away from the fixed point, space is divided into regions delineated by the largest real part. For example, consider the stability diagram shown in Figure 9. Domains of linear stability as a function of the mixing coefficient and the maximum grazing rate are shown in black and are characterized by eigenvalues whose real parts are negative; an unstable domain in which at least one eigenvalue has a positive real part is shown in white. The macrozooplankton parameters have been used, except for the variable grazing rate. Notice that for some grazing levels, stable regions are bracketed by unstable regions for different levels of the diffusivity. Although the examples analyzed above show a rather monotonic influence of diffusion, this plot shows that in fact it can be nonmonotonic. The analysis reveals linearly stable dynamics at some levels of mixing, but predicts unstable motion at others. This is particularly true for a grazing rate of, for example, 3.5/day which cross stability boundaries more than once as the diffusion is increased.

ii. Chaos. Although several measures of the dynamics of nonlinear systems exist, a critical one is the calculation of the Lyapunov exponent. This quantity measures the average exponential divergence rate of adjacent trajectories within a dynamical system and a positive exponent is a characteristic signature of chaos in the system. The method through

which this quantity is estimated has been described by several authors; one clear explanation is given by Wolf *et al.* (1985). A fiducial trajectory is calculated according to the complete, nonlinear set of equations. The Lyapunov spectrum is determined by integrating an orthonormal basis set through the linearized dynamics as determined along the fiducial course. Over the course of the linearized integration, vectors are rotated, stretched and contracted to the point where machine precision is reached. To avoid such numerical limitations the vector set is periodically reorthonormalized using the Gram-Schmidt procedure. Our approach follows the spirit of this description, though only the largest exponent is calculated, and renormalization occurs at every time step.

The Lyapunov exponent is calculated using a vertical resolution of 1 m, a full depth of 65 m, and a time step of 0.01 day. Trajectories are integrated for 3×10^5 days. Qualitative agreement after only 10^5 days of integration is excellent, with most exponents that are not approximately zero differing by only a few percent. Selected sensitivity analyses using a time step of 0.005 days also show good agreement with exponents presented below.

Figure 10 presents the exponent as a function of mixing coefficient for both the macrozooplankton (panel a) and microzooplankton (panel b) parameterizations. This exponent is positive for both models with quite weak diffusivities. Thus a chaotic attractor does exist for the diffusively coupled second-order system, but not in the range of realistic oceanic mixing levels. The largest of the exponents for the macrozooplankton model occurs for $K_v \sim 6.7 \times 10^{-8}$ m^2/s and has a value of approximately 0.003 day^{-1}. The microzooplankton model maximum exponent is found at a slightly larger diffusivity ($K_v \sim 1.7 \times 10^{-7}$ m^{-2}/s) but its maximum is nearly an order of magnitude larger ($\lambda_{max} \sim 0.025$ day^{-1}). The Lyapunov exponent also provides a measure of predictability for the system. This time scale depends on the accuracy of the initial conditions. For example, initial conditions known to within 1 part in 8 (i.e., 3 bits or $\sim$10%) have minimum predictability time scales of roughly 3 years for the macrozooplankton model as compared to roughly 4 months for the microzooplankton.

For realistic ocean levels of mixing, above 10^{-5} m^2/s, the largest Lyapunov exponent in the macrozooplankton model is negative, indicative of a stable fixed point solution and in agreement with the linear stability analysis presented above. Indeed, in the Lyapunov calculation, the transition to stable dynamics occurs very near to the critical value of 3.9×10^{-7} m^2/s mentioned previously. In contrast, the microzooplankton model shows a nearly zero exponent for realistic ocean diffusivities, indicative of a periodic attractor or other motion on a surface. This result is also consistent with the linear stability analysis conclusion that for large diffusivities, the many unstable modes of the microzooplankton model couple, coalesce and phase-lock in the vertical leading to a single oscillation over a large portion of the water column.

4. Summary and biological implications

The dynamics of a vertically-extended *NPZ* model subject to diffusive physics has been examined for two sets of biological parameters and a range of diffusivities. The biological

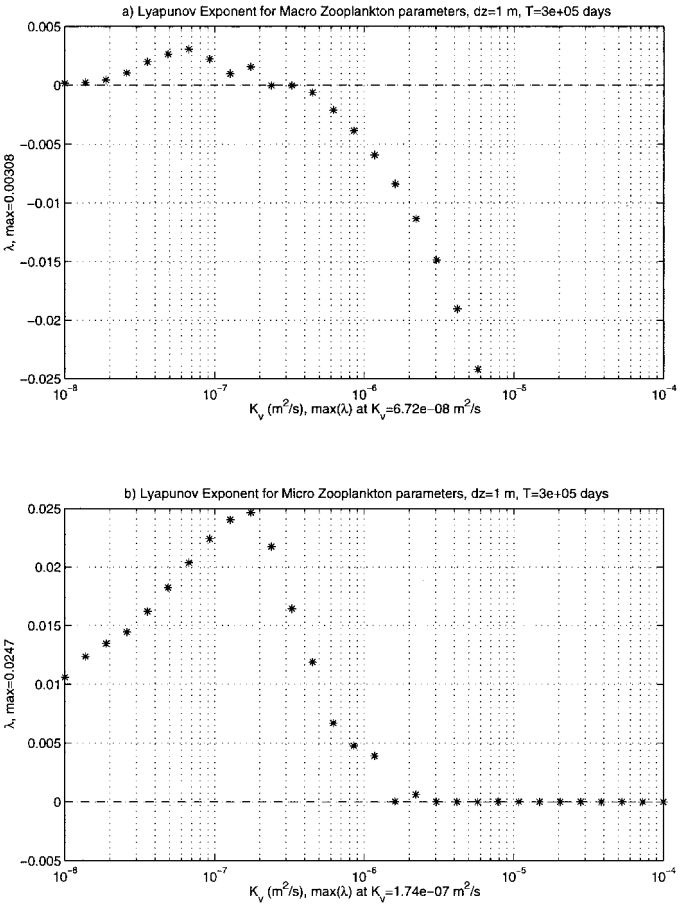

Figure 10. The largest Lyapunov exponent for (a) the macrozooplankton and (b) the microzooplankton parameterizations as a function of the vertical mixing coefficient.

dynamics depend on depth through the variable growth rate that decreases exponentially with depth due to light availability. When considered independently from the physics in the limit of zero diffusion, the biological model exhibits the expected characteristics of second-order dynamical systems, namely stable fixed points and limit cycle behavior, though this behavior does vary with depth, even for a constant set of parameters (Table 2). For parameters typical of macrozooplankton grazing and ingestion rates, the steady solution to the model is stable for depths less than roughly 25 m, unstable in the mid-portion of the water column ($-25\text{ m} > z > -50\text{ m}$), and again stable below 50 m, where the light limitation is so severe that the fixed point solution has zero phytoplankton and zooplankton concentrations. Using microzooplankton parameters reveals limit cycles that persist for all depths for which the phytoplankton population is nonzero. In both cases,

the oscillations that result in the biologically unstable portions of the water column have minimum periods of roughly 25 days nearest to the surface, increasing with depth.

The addition of sufficient diffusion to the system stabilizes the water column in the case of the macrozooplankton. This transition occurs at a $K_v \sim 4 \times 10^{-7}$ m^2/s, significantly below the diffusivities associated with even background levels of mixing. At weak but realistic levels ($K_v = 10^{-5}$ m^2/s), arbitrary initial conditions eventually lead to stable fixed points at all depths. Biological quantities oscillate at those depths that are unstable at lower diffusivities, but ultimately return to their steady-state values. For stronger levels of mixing, for example associated with wind-forced mixed layers, the oscillations are eliminated. In contrast, the microzooplankton parameter model maintains a fixed point solution that is unstable for even large mixing levels. Oscillations at different depths merge as the diffusivity is increased, until ultimately the growth and decay of biological fields within the entire water column are phase-locked.

Calculations of the largest Lyapunov exponent show that, consistent with the predator-prey model studied by Pascual (1993), the Franks *et al.* (1986) model is chaotic when a spatial dimension is added, with variable growth rate, and adjacent oscillators are coupled by diffusion. The more unstable nature of the nondiffusive microzooplankton model manifests itself through a Lyapunov exponent that is nearly 10 times larger than that calculated for the microzooplankton model. However, the chaotic motion is largest only for extremely weak diffusivities $O(10^{-7}$ m^2/s), and would not be observed in model applications using more realistic levels. The observation of chaos within real pelagic ecosystems remains inconclusive. While the analysis of a diatom time series from the Scripps pier revealed signatures of chaotic dynamics (Sugihara and May, 1990), analysis of net zooplankton and net phytoplankton biomass from a Middle Atlantic Bight mooring could neither support nor refute chaotic dynamics (Ascioti *et al.,* 1993). Within models, it is well known that systems of more than two dynamical variables can exhibit chaos, but its presence as a result of diffusion is less explored. In the present model it is not surprising that large diffusivities, which homogenize the upper water column on very short time scales, induce biological dynamics that are nearly spatially independent, and therefore not chaotic. However, it is less obvious that even background levels of mixing in the ocean would be sufficient to prevent chaos.

Our microzooplankton and macrozooplankton results have several implications for ecosystems in the real ocean. The *NPZ* model parameterized for microzooplankton has a one-dimensional fixed point profile very unlike those of the macrozooplankton parameterization (compare Figures 1 and 3 for the no-diffusion case). Steady solutions for the macrozooplankton model indicate near-surface depletion of nutrients, a strong nutricline, and relatively large surface concentrations of phytoplankton and zooplankton. These distributions are what one observes during late spring and summer in temperate regions. In marked contrast, the microzooplankton scenario has steady solutions that indicate very low phytoplankton and zooplankton at all depths, with most of the system nitrogen in the dissolved form. This is similar to high nutrient low chlorophyll (HNLC) regions such as the

Equatorial Pacific, Subarctic Pacific, and Southern Ocean (Barber and Chavez, 1991). Although the fixed point patterns are reminiscent of real observations for these HNLC regions, the extreme variability in the temporal dynamics as represented by Figure 4 (or as described in the text for the diffusive microzooplankton case) suggests inconsistencies between the model and present understanding of real dynamics in those regions. Of course, there may be other factors, such as iron (Martin *et al.,* 1991; Price *et al.,* 1991), that limit uptake in those regions but are not included in this model.

In addition, our results highlight more generally the important role played by physical processes influencing biological phenomena. The connection between levels of vertical mixing to plankton production processes is well known (see, e.g., Denman and Gargett, 1983). However, accounting for depth-integrated productivity allows only quantitative changes to biological fields as a result of varying mixed-layer depths. We have inquired how mixing generally affects ecosystem dynamics even at low diffusivities and have shown that mixing can stabilize vertical profiles, or not, depending on the conditions. Furthermore, we have illustrated how this influence can be nonmonotonic. For example, simply doubling the maximum grazing rate of the macrozooplankton parameter set leads to stable dynamics at background levels of mixing, but cyclic behavior throughout the water column at much higher, but still realistic mixing levels. Thus model dynamics are influenced qualitatively as well as quantitatively by diffusive processes. Our macrozooplankton results suggest that during seasons of weak mixing, or shallow mixed-layer depths during periods of strong insolation, one might anticipate that biological quantities, or those below the mixed layer, approach steady values on long, oscillatory routes. In contrast, during more actively forced periods, one might expect increasing variability at all depths. Obviously the biological dynamics subject to time-dependent forcing (i.e., driven by natural fluctuations of surface forcing) are significantly more complicated than those examined here. Nonetheless, considering changes in mixing levels on time scales long compared to biological changes (e.g., on seasonal time scales) as we have done here leads to interesting changes in biological dynamics. Our results also impact ecosystem interpretations on short time scales. Macrozooplankton model fluctuations (beyond the initial phytoplankton bloom) occur on the order of tens of days and therefore suggest that local, purely biological oscillations may be irrelevant when compared with faster advectively-induced responses. An example is the case of tidal motion considered by Franks and Chen (1996). Blooms modeled over tidal periods more clearly reflect direct response to physical forcing due simply to this clear separation of time scales.

Finally, our techniques are relevant to other modeling efforts, particularly since coupled biological-physical models are increasingly found in biological investigations (e.g., Lynch *et al.,* 1998). Conclusions from similar linear stability analyses promise to be useful in anticipating and interpreting large, coupled model results in these more complicated settings. A first example might be in the arena of model utilization. It is common practice to initialize biological models with conditions satisfying the time-independent equations. It would be valuable to know whether this solution represents a set of conditions that might

occur in the ocean given sufficient quiescence, or if in fact the initial condition is merely a special case in which the biological terms in the model formulations cancel, but otherwise do not attract biological concentrations. We note here that one limitation of the analysis of Section 2 is that it calculates only the linear stability. In the nonlinear system conditions that lie far from a stable fixed point may not evolve to the steady solution, but may instead approach a limit cycle (Strogatz, 1994). However, the linear analysis often provides excellent guidance as demonstrated in both the macrozooplankton and microzooplankton examples above. In addition, the long-term behavior of the ecosystem will of course vary considerably, simply based on the stability properties of the coupled biology and physics. For example, it is not unusual for *NPZ*-type models to produce transient phytoplankton blooms following the injection of nutrient-rich waters into the euphotic zone. However, the subsequent response might take one of two forms. Our model study has shown that such an injection can result in a short-lived increase in zooplankton, followed by periodic resurgence of this sequence, or a slow return to a stable solution that persists through time. Thus modeled ecosystem behavior can be interpreted through the understood dynamics of the steady solution. These implications are explored more thoroughly in the work by Edwards *et al.* (2000) who apply the present model within an idealized upwelling circulation.

Purposely, we have focused on the dynamics of among the simplest of ocean ecosystem models. Although there exists only a limited set of responses of the purely biological model, the spatially extended and diffusively coupled system exhibits a wider range of behavior and is very parameter dependent. It remains to be seen how the stability properties of the more complicated multi-component biological models will be modified by advection and diffusion, though both its stabilizing and destabilizing effects should be expected.

Acknowledgments. We are grateful to Peter Franks for many helpful comments and to Mercedes Pascual for aid in the calculation of the Lyapunov exponent. This research was supported by NSF Grant OCE-9618173 and is contribution no. 130 of the U.S. GLOBEC program, funded jointly by NSF and NOAA.

REFERENCES

Ascioti, F. A., E. Beltrami, T. O. Caroll and C. Wirick. 1993. Is there chaos in plankton dynamics? J. Plank. Res., *15,* 603–617.

Banse, K. 1992. Grazing, temporal changes of phytoplankton concentrations, and the microbial loop in the open sea, *in* Primary Productivity and Biogeochemical Cycles in the Sea, P. G. Falkowski and A. D. Woodhead, eds., Plenum Press, 249–258.

Barber, R. T. and F. P. Chavez. 1991. Regulation of primary productivity rate in the equatorial Pacific. Limnol. Oceanogr., *36,* 1803–1815.

Busenberg, S., S. K. Kumar, P. Austin and G. Wake. 1990. The dynamics of a model of plankton-nutrient interaction. Bull. Math. Biol., *52,* 677–696.

Denman, K. L. and A. E. Gargett. 1983. Vertical mixing and advection of phytoplankton in the upper ocean. Limnol. Oceanogr., *28,* 801–815.

—— 1995. Biological-physical interactions in the upper ocean. Ann. Rev. Fluid Mech., *27,* 225–255.

Doney, S. C., D. M. Glover and R. G. Najjar. 1996. A new coupled, one-dimensional biological-physical model for the upper ocean: Applications to the JGOFS Bermuda Atlantic Time-Series Study (BATS) site. Deep-Sea Res., *43,* 591–624.

Edwards, C. A., H. P. Batchelder and T. M. Powell. 2000. Modeling microzooplankton and macrozooplankton dynamics within a coastal upwelling system. J. Plankton Res. (in press).

Edwards, C. A. and J. Pedlosky. 1998. Dynamics of nonlinear cross-equatorial flow. Part II: The tropically enhanced instability of the western boundary current. J. Phys. Oceanogr., *28,* 2407–2417.

Fasham, M. J. R., H. W. Ducklow and S. M. McKelvie. 1990. A nitrogen-based model of plankton dynamics in the oceanic mixed layer. J. Mar. Res., *48,* 591–639.

Franks, P. J. S. 1997. New models for the exploration of biological processes at fronts. ICES J. Mar. Sci., *54,* 161–167.

Franks, P. J. S. and C. Chen. 1996. Plankton production in tidal fronts: A model of Georges Bank in summer. J. Mar. Res., *54,* 631–651.

Franks, P. J. S. and L. J. Walstad. 1997. Phytoplankton patches at fronts: A model of formation and response to wind events. J. Mar. Res., *55,* 1–29.

Franks, P. J. S., J. S. Wroblewski and G. R. Flierl. 1986. Behavior of a simple plankton model with food-level acclimation by herbivores. Marine Biology, *91,* 121–129.

Gifford, D. J. 1988. Impact of grazing by microzooplankton in the northwest arm of Halifax Harbour, Nova Scotia. Mar. Ecol. Prog. Ser., *47,* 249–258.

Hastings, A. and T. M. Powell. 1991. Chaos in a three species food chain. Ecology, *72,* 896–903.

Lynch, D. R., W. C. Gentleman, D. J. McGillicuddy Jr. and C. S. Davis. 1998. Biophysical simulations of *Calanus finmarchicus* population dynamics in the Gulf of Maine. Mar. Ecol. Prog. Ser., *169,* 189–210.

Martin, J. H., R. M. Gordon and S. E. Fitzwater. 1991. The case for iron. Limnol. Oceanogr., *36,* 1793–1800.

Moisan, J. R. and E. E. Hofmann. 1996. Modeling nutrient and plankton processes in the California coastal transition zone. 1. A time- and depth-dependent model. J. Geophys. Res., *101,* 22647–22676.

Neuer, S. and T. J. Cowles. 1994. Protist herbivory in the Oregon upwelling system. Mar. Ecol. Prog. Ser., *113,* 147–162.

Pascual, M. 1993. Diffusion-induced chaos in a spatial predator-prey system. Proc. R. Soc. Lond. B, *251,* 1–7.

Polzin, K. L., J. M. Toole, J. R. Ledwell and R. W. Schmitt. 1997. Spatial variability of turbulent mixing in the abyssal ocean. Nature, *276,* 93–96.

Price, N. M., L. F. Andersen and F. M. M. Morel. 1991. Iron and nitrogen nutrition of equatorial Pacific plankton. Deep-Sea Res., *96,* 1361–1378.

Sarmiento, J. L., D. Slater, M. J. R. Fasham, H. W. Ducklow, J. R. Toggweiler and G. T. Evans. 1993. A seasonal three-dimensional model of nitrogen cycling in the North Atlantic euphotic zone. Global Biogeochem. Cycles, *7,* 417–450.

Straile, D. 1997. Gross growth efficiencies of protozoan and metazoan zooplankton and their dependence on food concentration, predator-prey weight ratio, and taxonomic group. Limnol. Oceanogr., *42,* 1375–1385.

Strogatz, S. H. 1994. Nonlinear Dynamics and Chaos, Addison-Wesley, 498 pp.

Strom, S. L. and T. A. Morello. 1998. Comparative growth rates and yields of ciliates and heterotrophic dinoflagellates. J. Plank. Res., *20,* 571–584.

Sugihara, G. and R. M. May. 1990. Nonlinear forecasting as a way of distinguishing chaos from measurement error in time series. Nature, *344,* 734–741.

Sverdrup, H. U. 1953. On conditions for the vernal blooming of phytoplankton. J. Cons. Explor. Mer., *18,* 287–295.

Toole, J. M., K. L. Polzin and R. W. Schmitt. 1994. Estimates of diapycnal mixing in the abyssal ocean. Nature, *264,* 1120–1123.

Verity, P. G., D. K. Stoecker, M. E. Sieracki and J. R. Nelson. 1993. Grazing, growth and mortality of microzooplankton during the 1989 North Atlantic spring bloom at 47N, 18W. Deep-Sea Res. I, *40,* 1793–1814.

Wolf, A., J. B. Swift, H. L. Swinney and J. A. Vastano. 1985. Determining Lyapunov exponents from a time series. Physica D, *16,* 285–317.

Wroblewski, J. S. 1977. A model of phytoplankton plume formation during variable Oregon upwelling. J. Mar. Res., *35,* 357–394.

Wroblewski, J. S., J. L. Sarmiento and G. R. Flierl. 1988. An ocean basin scale model of plankton dynamics in the North Atlantic 1. Solutions for the climatological conditions in May. Global Biogeochem. Cycles, *31,* 199–218.

Received: *29 June, 1999;* revised: *7 December, 1999.*